JOURNAL OF AIRCRAFT
Vol. 47, No. 2, March–April 2010

Optimization of Active Flow Control over an Airfoil Using a Surrogate-Management Framework

Z.-H. Han,* K.-S. Zhang,† W.-P. Song,‡ and Z.-D. Qiao§
Northwestern Polytechnical University, 710072 Xi'an, People's Republic of China

DOI: 10.2514/1.45899

An efficient method based on the surrogate-management framework has been excised to optimize the actuation parameters of active flow control over an airfoil via a synthetic jet. In this approach, sample points are chosen by the design of experiments method, and approximation models are built based on the sampled data obtained from unsteady Reynolds-averaged Navier–Stokes simulations. The accuracy of these approximation models is evaluated at some test points by comparing the approximated values with the accurate values obtained from unsteady Reynolds-averaged Navier–Stokes simulations. Three types of approximation models (quadratic response-surface model, kriging model, and radial-basis-function neutral network) are built from the same data set. The model with highest accuracy is chosen as the surrogate model to be used to replace the unsteady Reynolds-averaged Navier–Stokes analysis during optimization. The optimization objective is to maximize the lift coefficient of a NACA 0015 airfoil at given angles of attack (14 to 22°), with the jet momentum coefficient, nondimensional frequency, and jet angle being the design variables. The surrogate model is coupled with a simulated annealing genetic algorithm optimizer to efficiently obtain the global optimum. As a result of the optimization process, the lift coefficient at an angle of attack of 16° is increased by 16.9% and the corresponding drag is decreased by 13.4% with respect to the initial controlled flow. It is preliminarily shown that the presented method is efficient and applicable for optimization of active flow control via a synthetic jet.

I. Introduction

ACTIVE flow control has received increasing attention from the researchers in the fluid dynamics community [1] during the past two decades. Innovative actuators such as synthetic jets [2] have the potential to dramatically improve the aerodynamic performance of some practical configurations. A synthetic jet is a zero-mass-flux device that can convert the electrical energy to the momentum injected into the main flow. This momentum injection without an air-mass source can result in similar control effect as the unsteady mass injection with an air-source system. A number of experimental and numerical studies demonstrated that a synthetic jet is promising in the context of active flow control applications such as separation control [3–8], thrust vectoring [9], mixing enhancement [10], virtual aero-shaping [11], forebody vortex control [12], active flow controls over helicopter rotors [13–15] and unmanned aerial vehicles [16], etc.

In recent years, the numerical simulation of aerodynamic stall control over an airfoil via a synthetic jet has received considerable attention [8,15,17–19]. The reason for this popularity can be explained by the fact that numerical simulation is an efficient way to evaluate the feasibility of synthetic jets for future application in full-scale aircraft. For the simulation of synthetic-jet flow control, large eddy simulation and direct numerical simulation are obviously more appropriate for resolving the small vortex structure induced by a synthetic jet [20]. However, the extremely high computational cost makes them still impractical for the simulation of high-Reynolds-number flows. Actually, most of the numerical simulations of active stall control via a synthetic jet were conducted by solving unsteady Reynolds-averaged Navier–Stokes (URANS) equations. The overall control effect observed in experiment was quite well reproduced by the URANS simulations. In addition to reproducing the physical phenomena of flow control via a synthetic jet, the numerical simulation also aims at optimizing the actuation parameters for an efficient control. The optimization of the actuation frequency and peak velocity of a synthetic jet for active flow control over a NACA 0012 airfoil were performed in [20] using a URANS flow solver and a gradient-based optimization algorithm. More recently, optimizing the control parameters (momentum coefficient, frequency, and angle with respect to the wall) of a synthetic jet for the stall control over a NACA 0015 airfoil was implemented in [21,22]. The optimizations were performed by coupling an automatic optimization algorithm with a time-accurate URANS flow solver. Each optimization took about 100 h of elapsed time using 16 processors (1600 h total CPU time). A significant improvement of the control efficiency was observed (maximum lift increased of 34% and stall delayed from 19 to 22° with respect to the initial controlled flow). This optimization methodology was further applied to optimization of the location of a synthetic jet on the suction side of a NACA 0012 airfoil in [23].

For the actuation-parameter optimization of active flow control over an airfoil via a synthetic jet, it is relatively more difficult than the commonly seen aerodynamic shape optimization of an airfoil. The difficulty is mainly caused by two facts:

1) The time-accurate simulation of synthetic-jet control is very time-consuming. Taking the simulation using a dual-time-stepping method as an example, at least 30 periods of unsteady simulations are usually needed to obtain a fully periodic solution. Supposing there are 100 physical time steps in one period of the synthetic-jet actuation and 100 subiterations for each physical time step, at least 300,000 iterations are generally necessary for a single simulation. The computational cost for a single simulation for flow control via a synthetic jet is at least 300 times higher than a single steady simulation for aerodynamic-shape optimization. Hence, the total CPU time needed for optimizing such an active flow control could be prohibitively

Presented as Paper 1280 at the 47th AIAA Aerospace Sciences Meeting, Orlando, FL, 5–8 January 2009; received 8 June 2009; revision received 6 December 2009; accepted for publication 21 December 2009.

*Lecturer, National Key Laboratory of Aerodynamic Design and Research, School of Aeronautics, P.O. Box 754, School of Aeronautics, No. 127 West Youyi Roadn; hanzh@nwpu.edu.cn.

†Associate Professor, National Key Laboratory of Aerodynamic Design and Research, School of Aeronautics, P.O. Box 120, School of Aeronautics, No. 127 West Youyi Road; zhangkeshi@nwpu.edu.cn.

‡Professor, National Key Laboratory of Aerodynamic Design and Research, School of Aeronautics, P.O. Box 754, School of Aeronautics, No. 127 West Youyi Road; wpsong@nwpu.edu.cn.

§Senior Professor, National Key Laboratory of Aerodynamic Design and Research, School of Aeronautics, P.O. Box 754, School of Aeronautics, No. 127 West Youyi Road; zdqiao@nwpu.edu.cn.

unacceptable if the time-accurate simulation is executed at every step of optimization.

2) To improve the efficiency of optimization, gradient-based algorithm is often preferable. However, the optimization may converge to a local optimum when using a gradient-based optimization algorithm. A genetic algorithm (GA), an evolutionary algorithm, is a gradient-free method and well suitable for global optimization. However, it is much more expensive. Therefore, GA is only used for the aerodynamic shape optimization with low-fidelity and efficient computational fluid dynamics (CFD) computations. Direct coupling of GA and time-accurate high-fidelity CFD for optimization of active flow control via a synthetic jet is prohibitive due to the extremely high computational cost.

This paper is motivated by the development of an efficient approach to address the high computational cost associated with the optimization of active stall control via a synthetic jet. In this approach, the design of experiments (DOE) method is used to select sample points in the design space. Then URANS simulations are performed to obtain the aerodynamic data at these samples. Different types of approximation models such as the quadratic response-surface model (RSM), kriging, and radial-basis-function neutral network (RBF-NN) are built based on the sampled data. Error estimation is performed for each approximation model and the best model is chosen as the surrogate model to be used in optimization, under the condition that the approximation accuracy satisfies the requirement of a designer. As the time-consuming CFD analysis is completely replaced by an efficient surrogate model, it is possible to use a global optimization method such as GA to obtain the global optimum. In this study, a simulated annealing genetic algorithm (SAGA) was employed, and very high efficiency has been obtained when it was coupled with the surrogate-management framework. The developed method was applied to the actuation-parameter optimization of a synthetic jet for active flow control over a NACA 0015 airfoil. The feasibility and efficiency of using this method were evaluated and demonstrated.

II. Numerical Simulation Methods

An in-house CFD code developed by the authors was used for the time-accurate numerical simulations associated to the active flow control over an airfoil via a synthetic jet. After introducing a pseudo-time-derivative term, an integral form of the preconditioned 2-D compressible URANS equations can be written as

$$\iint_{\Omega}\int \boldsymbol{P}\frac{\partial \boldsymbol{W}}{\partial \tau}\,\mathrm{d}V + \iint_{\Omega}\int \frac{\partial \boldsymbol{W}}{\partial t}\,\mathrm{d}V + \iint_{\partial\Omega} \bar{\bar{\boldsymbol{H}}}\cdot\boldsymbol{n}\,\mathrm{d}S = \iint_{\partial\Omega} \bar{\bar{\boldsymbol{H}}}_{v}\cdot\boldsymbol{n}\,\mathrm{d}S \tag{1}$$

where $\boldsymbol{W} = (\rho, \rho u, \rho v, \rho e)^T$ denote the conservative variables; $\boldsymbol{P}$ is the preconditioning matrix; $\bar{\bar{\boldsymbol{H}}}$ and $\bar{\bar{\boldsymbol{H}}}_v$ denote the inviscid and viscous flux vectors, respectively; t and τ are the physical and pseudo time, respectively. Note that the preconditioning matrix $\boldsymbol{P}$ is imposed on the pseudo-time-derivative term to ensure the time-accurate solution.

For the CFD code, the control equations are solved by a cell-centered finite volume scheme. An AUSM$^+$-up scheme proposed by Liou [24] are used for spatial discretization, and a fully implicit dual-time-stepping method with Newton-like lower–upper symmetric Gauss–Seidel subiteration is implemented for time integration. The fully turbulent flow is assumed for all the simulations. The turbulence viscous coefficient is calculated by the Spalart–Allmaras one-equation turbulence model. To improve the efficiency and robustness of the compressible CFD code for low-speed flows or flows with a low-speed-flow region, a preconditioning method proposed by Turkel et al. [25] is implemented within the framework of a full-approximation-storage multigrid method. Although the AUSM$^+$-up scheme already specially considers the dissipation of spatial discretization for low-speed flows, it was found that the efficiency for the low-speed flows can be further improved when it is combined with a low-speed preconditioning time-stepping scheme [26]. The detailed description about the numerical scheme can be found in [26–28].

To model the influence of a synthetic jet on the main flow over an airfoil, an unsteady blowing/suction boundary condition is imposed along the orifice of actuator (see Fig. 1). The prescribed velocity is

$$\boldsymbol{U}(\xi, 0, t) = U_m \sin(\omega_{\text{jet}} t) f(\xi)\boldsymbol{d}_{\text{jet}} \tag{2}$$

where U_m is the peak velocity of synthetic jet, ω_{jet} is the angular frequency, $\boldsymbol{d}_{\text{jet}}$ is a vector of unit length representing the direction of the jet outlet, θ_{jet} (called jet angle in the text below) is defined as the angle between the $\boldsymbol{d}_{\text{jet}}$ and the surface of the wall, and $f(\xi)$ represents the tangent-direction distribution of the jet velocity. Following [18], a top-hat distribution is adopted as

$$f(\xi) = 1 \tag{3}$$

assuming that the spatial variation of the tangent distribution has a negligible effect on the flow control. The nondimensional frequency of a synthetic jet is defined as

$$F^+ = \frac{\omega_{\text{jet}} x_{te}}{2\pi U_\infty} \tag{4}$$

where U_∞ is the freestream velocity and x_{te} is the distance between the location of a synthetic jet and the trailing edge of the airfoil. Note that F^+ represents the ratio of the time in which the flow past the airfoil and the period of actuation.

To describe the relative energy of a synthetic jet used for flow control, the momentum coefficient [3] is defined as

$$C_\mu = 2\frac{H}{c}\left(\frac{U_m}{\sqrt{2}U_\infty}\right)^2 \tag{5}$$

where H, the effective width of the synthetic jet, is defined as

$$H = \sin\theta_{\text{jet}} \cdot h \int_0^1 f^2(\xi)\,\mathrm{d}\xi$$

(where h is the width of a synthetic jet), and c is the chord length of the airfoil. Incorporating Eqs. (4) and (5) into Eq. (2) results in

$$\boldsymbol{U}(\xi, 0, t) = \sqrt{2c_u}\sin\left(\frac{2\pi U_\infty F^+}{c}t\right) f(\xi)\boldsymbol{d}_{\text{jet}} \tag{6}$$

In addition, the momentum relation in normal direction of the airfoil surface along the jet orifice is modified as

$$\frac{\partial p}{\partial \eta} = -\rho\frac{\partial U_n}{\partial t} \tag{7}$$

From Eq. (6), one can see that momentum coefficient, nondimensional frequency, and jet angle are three key parameters for flow control via a synthetic jet. They are taken as the design variables for the optimization problem in the next section.

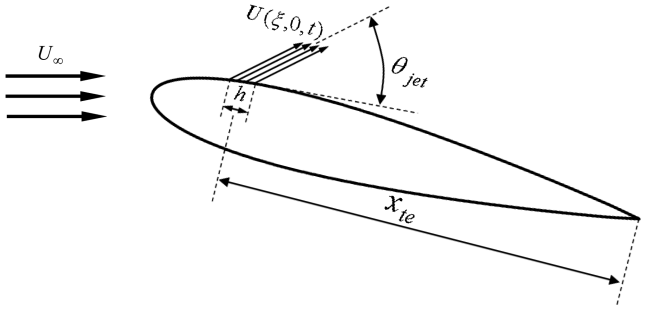

Fig. 1 Unsteady blowing/suction boundary condition imposed on an airfoil.

III. Optimization Method Based on a Surrogate-Management Framework

A method coupling the time-accurate URANS simulation and GA optimization within a surrogate-management framework has been developed for efficient optimization of actuation parameters of synthetic-jet flow control. Note that here the terminology *surrogate model* has the same meaning as *metamodel*, *response-surface model*, *approximation model*, or *emulator*. For surrogate-based optimization, one of the main challenges is related to the problem of size [29]. With the increase in the number of design variables, the computational cost related to building a usable surrogate model increases very quickly. However, for a problem with a number of design variables of less than 15, the computational cost is generally acceptable. For the optimization of actuating parameters of synthetic jet, there are only a few key parameters (see Sec. II), and the problem of size is beyond the scope of this paper.

The locations of sample points in design space are determined by the DOE method, and the approximation models are built from the sampled data obtained from the URANS simulations. During optimization, the complicated and time-consuming CFD analysis is replaced by a surrogate model with acceptable accuracy but much higher computational efficiency. The key points of the method are how to construct approximation models and how to manage these models to get a surrogate model that is adequate for optimization. The combination of several approximation methods (RSM [30], kriging [31–33], and RBF-NN [34,35]) is made, and the accuracy is assessed by an error-estimation procedure.

A. Design of Experiments

For surrogate modeling, DOE methods are usually used to determine the location of sample points in design space. DOE is a procedure for choosing a set of sample points, with the general goal of maximizing the amount of information gained from a limited number of sample points [36]. Currently, there are different DOE methods that can be classified into two categories: classic DOE methods and modern DOE methods [36]. The classic DOE methods such as full- and fractional-factorial design, central composite design, Box–Behnken, and *D*-optimal design were developed for the arrangement of laboratory experiments, with the consideration of reducing the effect of random error. The modern DOE methods such as Latin hypercube sampling, orthogonal array design, and quasi Monte Carlo sampling were developed for deterministic computer experiments without random error. A good overview of the modern DOE methods was presented in [36]. In addition to the DOE methods mentioned above, the uniform design (UD) method (see [37]), from the authors' points of view, should be also classified as a modern DOE method, as it was developed to address the requirements of computer experiments. UD has been widely used in various communities during the past three decades, which shows that it can generate uniform distributed sample points and that a relatively small number of sample points are generally required. In this study, the UD is employed in the demonstration of the developed method in the next section.

B. Approximation Models

RSM, kriging, and RBF-NN are known as the most popular approximation models that can be used as surrogates of the high-fidelity but expensive CFD codes.

Before the description of the approximation models used in this study, some necessary definitions are subsequently given. Assuming that there are N sample points for an N_v-dimensional problem, the sampled data sets $(\boldsymbol{X}_S, \boldsymbol{Y}_S)$ can be defined as shown here:

$$\boldsymbol{X}_S = \begin{bmatrix} \boldsymbol{x}_{S,1} \\ \boldsymbol{x}_{S,2} \\ \vdots \\ \boldsymbol{x}_{S,N} \end{bmatrix} = \begin{bmatrix} x_{S,1}^1 & x_{S,1}^2 & \cdots & x_{S,1}^{N_V} \\ x_{S,2}^1 & x_{S,2}^2 & \cdots & x_{S,2}^{N_V} \\ \vdots & \vdots & \cdots & \vdots \\ x_{S,N}^1 & x_{S,N}^1 & \cdots & x_{S,N}^{N_V} \end{bmatrix} \in \mathbb{R}^{N \times N_V},$$
$$\boldsymbol{Y}_S = \begin{bmatrix} y_{S,1} \\ y_{S,2} \\ \vdots \\ y_{S,N} \end{bmatrix} \in \mathbb{R}^N, \qquad \boldsymbol{x}_{S,i} \in \mathbb{R}^{N_V}, \qquad y_{S,i} \in \mathbb{R}^1 \tag{8}$$

where $\boldsymbol{X}_S$ is the design matrix, with each row vector representing a sample site, and $\boldsymbol{Y}_S$ is the column vector that contains the values of the response at each sample site. Note that the goal of building an approximation model is to get the response $\hat{y}$ at any untied $\boldsymbol{x}$ based on the observed data sets $(\boldsymbol{X}_S, \boldsymbol{Y}_S)$.

1. Quadratic Response Surface Method

Here, we use RSM to denote a polynomial approximation model in which the sampled data is fitted by a least-squares regression technique. In RSM-based optimization applications, the quadratic RSM usually provides the best compromise between the modeling accuracy and computational expense, when compared with the linear or higher-order polynomial models. An advantage of RSM is that it can be used to smooth out the various scales of numerical noise in the data while it captures the global trend of the variation. Another advantage of RSM is that it is easy to implement and inexpensive to use.

The true quadratic RSM can be written in the following form:

$$y(\boldsymbol{x}) = \hat{y}(\boldsymbol{x}) + \varepsilon, \qquad \boldsymbol{x} \in \mathbb{R}^{N_V} \tag{9}$$

where $y(\boldsymbol{x})$: $\mathbb{R}^{N_v} \to \in \mathbb{R}^1$ is the unknown function to be approximated, $\hat{y}(\boldsymbol{x})$ is the quadratic polynomial approximation, and ε is the random error assumed to be normally distributed with mean zero and variance of σ^2. The error ε_i at each observation is supposed to be an independent and identically distributed. RSM predictor$\hat{y}(\boldsymbol{x})$ can be written as

$$\hat{y}(\boldsymbol{x}) = \beta_0 + \sum_{i=1}^{N_V} \beta_i x_i + \sum_{i=1}^{N_V} \beta_{ii} x_i^2 + \sum_{1 \le i < j \le N_V}^{N_V} \beta_{ij} x_i x_j,$$
$$\boldsymbol{x} = (x_1, x_2, \ldots, x_{N_V})^T \in \mathbb{R}^{N_V} \tag{10}$$

where β_0, β_i, β_{ii}, and β_{ij} are unknown coefficients to be determined by the least-squares regression, with which the sum of the squared error is minimized. Since there are a total of $p = (N_V + 1)(N_V + 2)/2$ unknown coefficients in Eq. (10), building a quadratic RSM with N_V variables requires at least p sample points. Let $\boldsymbol{\beta} \in \mathbb{R}^p$ be the column vector that contains these p unknown coefficients. The least-squares estimator of $\boldsymbol{\beta}$ is

$$\boldsymbol{\beta} = (\boldsymbol{U}^T \boldsymbol{U})^{-1} \boldsymbol{U}^T \boldsymbol{Y}_S \tag{11}$$

where

$$\boldsymbol{U} = \begin{bmatrix} 1 & x_{S,1}^1 & x_{S,1}^2 & \cdots & x_{S,1}^{N_V} & x_{S,1}^1 x_{S,1}^2 & x_{S,1}^1 x_{S,1}^3 & \cdots & x_{S,1}^{N_V-1} x_{S,1}^{N_V} & (x_{S,1}^1)^2 & (x_{S,1}^2)^2 & \cdots & (x_{S,1}^{N_V})^2 \\ 1 & x_{S,2}^1 & x_{S,2}^2 & \cdots & x_{S,2}^{N_V} & x_{S,2}^1 x_{S,2}^2 & x_{S,2}^1 x_{S,2}^3 & \cdots & x_{S,2}^{N_V-1} x_{S,2}^{N_V} & (x_{S,2}^1)^2 & (x_{S,2}^2)^2 & \cdots & (x_{S,2}^{N_V})^2 \\ \vdots & \vdots & \vdots & \ddots & \vdots & \vdots & \vdots & \ddots & \vdots & \vdots & \vdots & \ddots & \vdots \\ 1 & x_{S,N}^1 & x_{S,N}^2 & \cdots & x_{S,N}^{N_V} & x_{S,N}^1 x_{S,N}^2 & x_{S,N}^1 x_{S,N}^3 & \cdots & x_{S,N}^{N_V-1} x_{S,N}^{N_V} & (x_{S,N}^1)^2 & (x_{S,N}^2)^2 & \cdots & (x_{S,N}^{N_V})^2 \end{bmatrix} \in \mathbb{R}^{N \times p} \tag{12}$$

After the unknown coefficients in $\boldsymbol{\beta}$ are determined, the approximated response $\hat{y}$ at any untried $\boldsymbol{x}$ can be efficiently predicted by Eq. (10).

2. *Kriging Model*

Different from RSM, kriging is an interpolating method in which the function values at sample points are exactly reproduced. Kriging provides a statistic prediction of response by minimizing its mean squared error (MSE). It can be equivalent to any order of polynomials and is well suited for highly nonlinear functions with multiple extremes. For the derivation of kriging, the output of a deterministic computer experiment is treated as a realization of a random function (or stochastic process), and then statistical techniques can be used to compute the MSE of the prediction. The readers are referred to [31] for the use of statistical techniques in the design and analysis of computer experiments. Here, $y(\boldsymbol{x})$ is treated as the sum of a global trend function $\boldsymbol{f}^T(x)\boldsymbol{\beta}$ and a Gaussian random function $Z(\boldsymbol{x})$:

$$y(\boldsymbol{x}) = \boldsymbol{f}^T(\boldsymbol{x})\boldsymbol{\beta} + Z(\boldsymbol{x}), \qquad \boldsymbol{x} \in \mathbb{R}^{N_V} \tag{13}$$

where $\boldsymbol{f}(\boldsymbol{x}) = \{f_0(\boldsymbol{x}), \ldots, f_{p-1}(\boldsymbol{x})\}^T \in \mathbb{R}^p$ is defined with a set of the regression functions and $\boldsymbol{\beta} = (\beta_0, \ldots, \beta_{p-1})^T \in \mathbb{R}^p$ denotes the corresponding coefficients. In general, $\boldsymbol{f}^T(\boldsymbol{x})\boldsymbol{\beta}$ is taken as either a constant or as low-order polynomials. In this study, a quadratic polynomial is employed as the trend function. In Eq. (13), $Z(\cdot)$ denotes a stationary random process with a zero mean, variance σ^2, and nonzero covariance:

$$\operatorname{cov}\{Z(\boldsymbol{x}), Z(\boldsymbol{x}')\} = \sigma^2 R(\boldsymbol{x}, \boldsymbol{x}') \tag{14}$$

Here, $R(\boldsymbol{x}, \boldsymbol{x}')$ is the correlation function that is only dependent on the Euclidean distance between any two sites $\boldsymbol{x}$ and $\boldsymbol{x}'$ in the design space.

From the derivation in [31], the kriging predictor $\hat{y}(\boldsymbol{x})$ for any untried $\boldsymbol{x}$ can be written as

$$\hat{y}(\boldsymbol{x}) = \boldsymbol{f}^T(\boldsymbol{x})\boldsymbol{\beta} + \boldsymbol{r}^T(\boldsymbol{x})\boldsymbol{R}^{-1}(\boldsymbol{Y}_S - \boldsymbol{F}\boldsymbol{\beta}) \tag{15}$$

where the generalized least-squares estimation of $\boldsymbol{\beta}$ is

$$\boldsymbol{\beta} = (\boldsymbol{F}^T\boldsymbol{R}^{-1}\boldsymbol{F})^{-1}\boldsymbol{F}^T\boldsymbol{R}^{-1}\boldsymbol{Y}_S \tag{16}$$

$\boldsymbol{F}$ is created by evaluating $\boldsymbol{f}(\boldsymbol{x})$ at each of the N known observations,

$$\boldsymbol{F} = \begin{bmatrix} \boldsymbol{f}(\boldsymbol{x}_{s,1}) \\ \boldsymbol{f}(\boldsymbol{x}_{s,2}) \\ \vdots \\ \boldsymbol{f}(\boldsymbol{x}_{s,N}) \end{bmatrix} \in \mathbb{R}^{N\times p} \tag{17}$$

and $\boldsymbol{R}$ and $\boldsymbol{r}$ are the correlation matrix and the correlation vector, respectively. $\boldsymbol{R}$ and $\boldsymbol{r}$ are defined as

$$\boldsymbol{R} = \begin{bmatrix} R(\boldsymbol{x}_{S,1}, \boldsymbol{x}_{S,1}) & R(\boldsymbol{x}_{S,1}, \boldsymbol{x}_{S,2}) & \cdots & R(\boldsymbol{x}_{S,1}, \boldsymbol{x}_{S,N}) \\ R(\boldsymbol{x}_{S,2}, \boldsymbol{x}_{S,1}) & R(\boldsymbol{x}_{S,2}, \boldsymbol{x}_{S,2}) & \cdots & R(\boldsymbol{x}_{S,2}, \boldsymbol{x}_{S,N}) \\ \vdots & \vdots & \ddots & \vdots \\ R(\boldsymbol{x}_{S,N}, \boldsymbol{x}_{S,1}) & R(\boldsymbol{x}_{S,N}, \boldsymbol{x}_{S,2}) & \cdots & R(\boldsymbol{x}_{S,N}, \boldsymbol{x}_{S,N}) \end{bmatrix} \in \mathbb{R}^{N\times N},$$

$$\boldsymbol{r} = \begin{bmatrix} R(\boldsymbol{x}_{S,1}, \boldsymbol{x}) \\ R(\boldsymbol{x}_{S,2}, \boldsymbol{x}) \\ \vdots \\ R(\boldsymbol{x}_{S,N}, \boldsymbol{x}) \end{bmatrix} \in \mathbb{R}^N \tag{18}$$

where $R(\boldsymbol{x}_{S,i}, \boldsymbol{x}_{S,j})$ denotes the correlation between any two observed points, and $R(\boldsymbol{x}_{S,i}, \boldsymbol{x})$ is the correlation between the observed point $\boldsymbol{x}_{S,i}$ and the untried point $\boldsymbol{x}$. In this study, a Gaussian correlation function is adopted, and it is of the form

$$R(\boldsymbol{x}_{S,i}, \boldsymbol{x}_{S,j}) = \exp\left[-\sum_{k=1}^{N_V} \theta_k (x_{S,i}^k - x_{S,j}^k)^2\right] \tag{19}$$

where $\boldsymbol{\theta} = (\theta_1, \theta_2, \ldots, \theta_{N_v})^T$ denotes the unknown correlation parameters (hyperparameters). In general, $\boldsymbol{\theta}$ is obtained by an optimization process with maximum likelihood estimation (see [33]). However, difficulties can sometimes be caused if the maximum of likelihood function always appears at the upper bound of $\boldsymbol{\theta}$ and if the design space for $\boldsymbol{\theta}$ is noisy. This paper uses an alternative (more robust) method for the optimization of $\boldsymbol{\theta}$. In this method, the objective is to find the best $\boldsymbol{\theta}$ to minimize the mean error of the kriging model being evaluated on test points (see the next subsection).

The MSE of the kriging predictor $\hat{y}(\boldsymbol{x})$ is of the form

$$\text{MSE}\{\hat{y}(\boldsymbol{x})\} = \sigma^2\left\{1.0 - \begin{bmatrix} \boldsymbol{r}(\boldsymbol{x}) \\ \boldsymbol{f}(\boldsymbol{x}) \end{bmatrix}^T \begin{bmatrix} \boldsymbol{R} & \boldsymbol{F} \\ \boldsymbol{F}^T & 0 \end{bmatrix}^{-1} \begin{bmatrix} \boldsymbol{r}(\boldsymbol{x}) \\ \boldsymbol{f}(\boldsymbol{x}) \end{bmatrix}\right\} \tag{20}$$

where

$$\sigma^2 = \frac{1}{N}(\boldsymbol{Y}_S - \boldsymbol{F}\boldsymbol{\beta})^T\boldsymbol{R}^{-1}(\boldsymbol{Y}_S - \boldsymbol{F}\boldsymbol{\beta}) \tag{21}$$

3. *Radial-Basis-Function Neutral Network*

Among different kinds of neutral networks, RBF-NN was frequently used to build an approximation model. RBF-NN takes the radial basis functions as the transfer functions in the neutral network. According to RBF-NN, the response at any untried $\boldsymbol{x}$ can be written as

$$y(\boldsymbol{x}) = \sum_{j=1}^{p} \lambda_j \varphi_j(\boldsymbol{x}) + \theta, \qquad \boldsymbol{x} \in \mathbb{R}^{N_V} \tag{22}$$

where p is the number of the hidden layers, φ_j is the transfer function of the jth hidden layer (it is taken here as a radial basis function), λ_j is the weighting coefficient, and θ is an unknown value. Note that the number of the hidden layers p is a parameter prescribed by the user. With larger p, $\hat{y}(\boldsymbol{x})$ will approach $y(\boldsymbol{x})$ more closely, but more sample points are required. The number of sample points N should be no less than p. The predicted value of the true response $y(\boldsymbol{x})$ at an untried point $\boldsymbol{x}$ is given by

$$\hat{y}(\boldsymbol{x}) = \sum_{j=1}^{p} \hat{\lambda}_j \varphi_j(\boldsymbol{x}) + \hat{\theta} \tag{23}$$

The unknown parameters in φ_j should be computed based on the sampled data. Various functions, such as Gaussian basis function, Gaussian bar function, thin plate spline, Hardy multiquadratics and Hardy inverse multiquadratics, etc., may act as the radial basis function. In this work, the Gaussian bar function is employed, due to its better characteristics in global approximation. It takes the form as

$$\varphi_p(\boldsymbol{x}) = \sum_{i=1}^{N_V} \exp\left[-\frac{1}{2}\left(\frac{x_i - c_{p,i}}{\sigma_{p,i}}\right)^2\right] \tag{24}$$

where, $\boldsymbol{c}_p = (c_{p,1}, \ldots, c_{p,N_V})$ is the center of φ_p, and $\boldsymbol{\sigma}_p = (\sigma_{p,1}, \ldots, \sigma_{p,N_V})$ is its variance. In this study, $\boldsymbol{c}_p$ is calculated by a K-means clustering method. First, any p sample points are defined as the centers. Here, the first p sample points are chosen, i.e., $\{\boldsymbol{c}_p\}_{i=1}^p = \{\boldsymbol{x}_{Si}\}_{i=1}^p$. Second, all sample points are grouped with their nearest center points. Third, the mean value at all the sample points in the same group is calculated and then acts as the new center of that group. If the new center and the old center are close enough, the K-means clustering process terminates. The variance is given as

$$\sigma_{p,i}^2 = \frac{d_{\max,i}^2}{2p}, \qquad i \in \{1, 2, \ldots, N_V\} \tag{25}$$

where $d_{\max,i}$ is the maximum distance between any two centers of φ_p.

In Eq. (23), the unknown coefficients $\hat{\lambda}_j$ and $\hat{\theta}$ can be calculated by the least-squares regression technique as

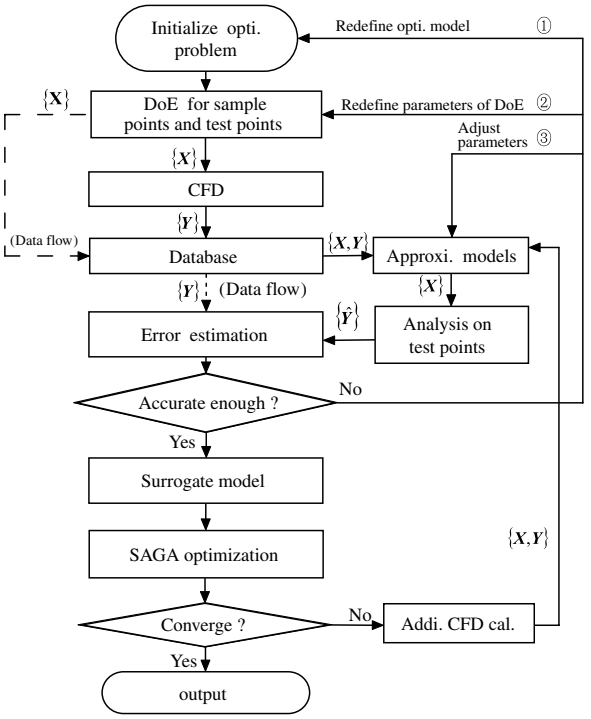

Fig. 2 Flowchart of surrogate-management framework (also see [38]).

$$[\hat{\lambda}_1, \hat{\lambda}_2, \ldots, \hat{\lambda}_p, \hat{\theta}] = (\boldsymbol{H}^T\boldsymbol{H})^{-1}\boldsymbol{H}^T\boldsymbol{Y}_S \tag{26}$$

where

$$\boldsymbol{H} = \begin{bmatrix} \varphi_1(\boldsymbol{x}_{S,1}) & \varphi_2(\boldsymbol{x}_{S,1}) & \cdots & \varphi_p(\boldsymbol{x}_{S,1}) & 1 \\ \varphi_1(\boldsymbol{x}_{S,2}) & \varphi_2(\boldsymbol{x}_{S,2}) & \cdots & \varphi_p(\boldsymbol{x}_{S,2}) & 1 \\ \vdots & \vdots & \ddots & \vdots & 1 \\ \varphi_1(\boldsymbol{x}_{S,N}) & \varphi_2(\boldsymbol{x}_{S,N}) & \cdots & \varphi_p(\boldsymbol{x}_{S,N}) & 1 \end{bmatrix} \tag{27}$$

C. Evaluation of Approximation Models

An important issue for the surrogate-based optimization is how to estimate the error of approximation models. Only when the surrogate model with sufficient accuracy is built can the reliable optimum be obtained. This paper uses two variables ($\bar{e}$ and σ_e) to evaluate the

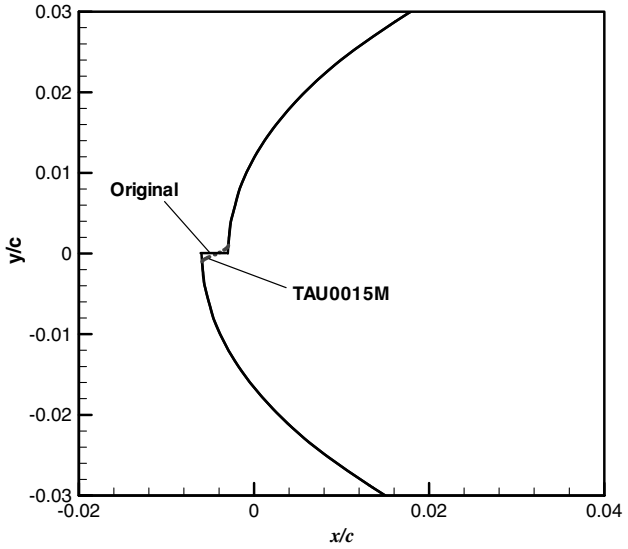

Fig. 3 Comparison of leading-edge shape of the original and modified TAU0015 airfoils.

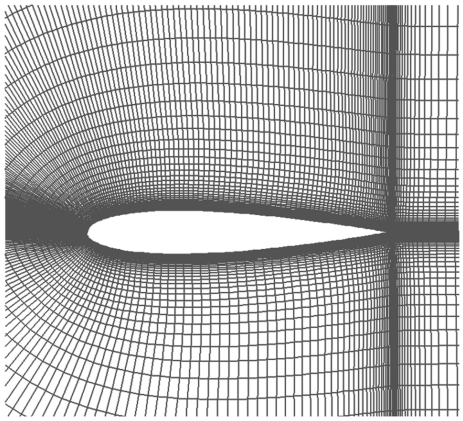

Fig. 4 Computational grid for simulation of flow control over a TAU0015 airfoil.

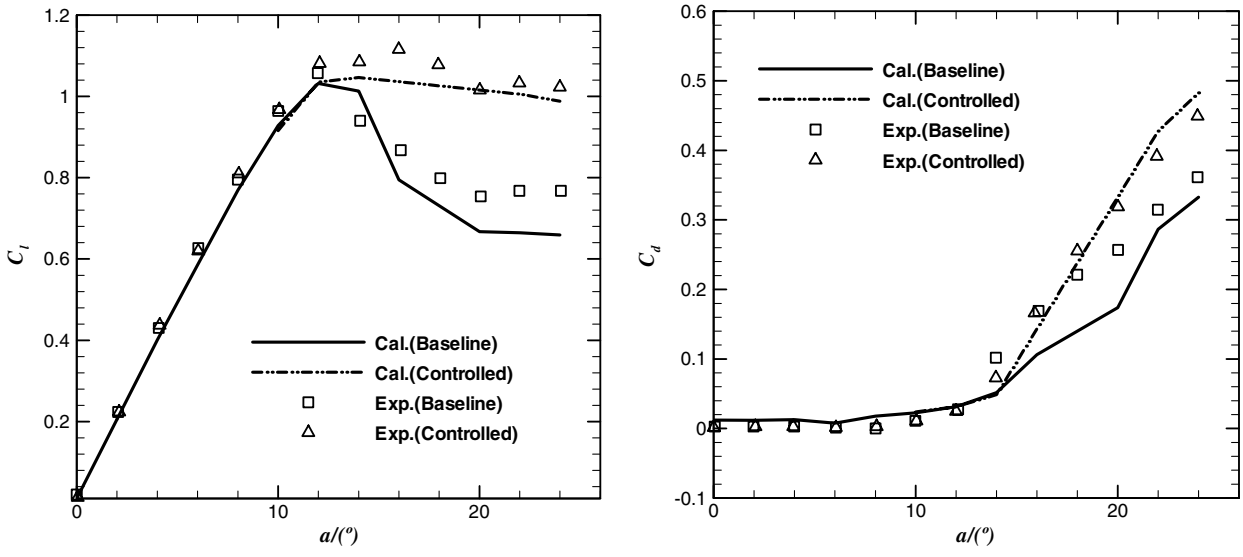

a) C_l-Vs.- α b) C_d-Vs.- α

Fig. 5 Comparisons of predicted results with experiment data for baseline and controlled cases of a TAU0015 airfoil ($Ma = 0.15$, $Re = 1.2 \times 10^6$, $C_u = 0.03\%$, and $F^+ = 0.58$).

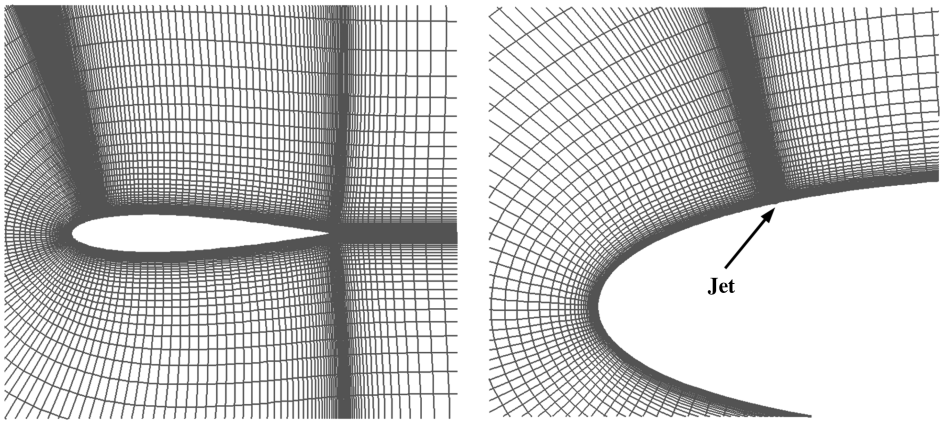

Fig. 6 Computational grid for simulation of flow control on a NACA 0015 airfoil.

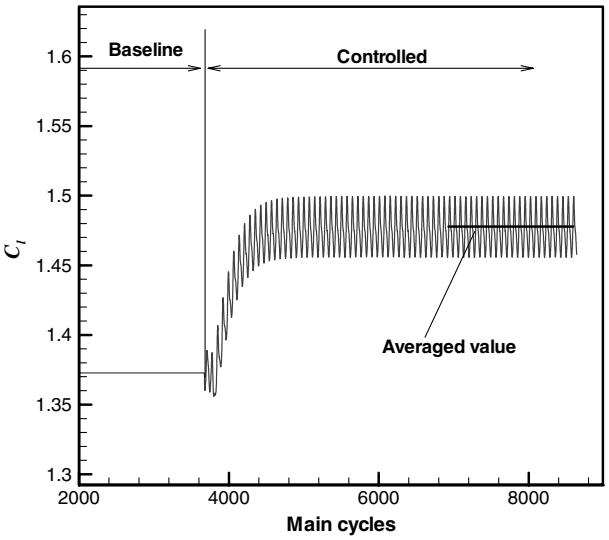

Fig. 7 Typical convergence history of lift coefficient during unsteady simulation of flow control over NACA 001 airfoil.

error of the approximation models at test points. Test points are also chosen by the DOE method. The average relative error is

$$\bar{e} = \frac{1}{N_{\text{test}}} \sum_{i=1}^{N_{\text{test}}} e_i, \qquad e_i = \left\| \frac{\hat{y}_{T,i} - y_{T,i}}{y_{T,i}} \right\| \tag{28}$$

Table 1 Control parameters for sample points

Sample point	C_μ	F^+	$\theta_{\text{jet}}/^\circ$.
1	0.01367	0.20000	10.00000
2	0.00100	0.63333	33.33333
3	0.00100	0.20000	33.33333
4	0.00733	0.63333	45.00000
5	0.02000	0.20000	21.66667
6	0.01367	0.63333	21.66667
7	0.02000	1.06667	45.00000
8	0.00733	1.50000	10.00000
9	0.00100	0.63333	10.00000
10	0.01367	0.20000	45.00000
11	0.02000	1.06667	10.00000
12	0.01367	1.06667	33.33333
13	0.00733	0.20000	21.66667
14	0.00100	1.50000	21.66667
15	0.00733	1.50000	45.00000
16	0.00733	1.06667	10.00000
17	0.01367	1.50000	33.33333
18	0.00100	1.06667	45.00000
19	0.02000	1.50000	21.66667
20	0.02000	0.63333	33.33333

where N_{test} is number of the test points, and $y_{T,i}$ and $\hat{y}_{T,i}$ are, respectively, the true value and predicted value corresponding to the ith test point. The root-mean-squared error is defined as

$$\sigma_e = \sqrt{\sum_{i=1}^{N_{\text{test}}} \frac{e_i^2}{N_{\text{test}}}} \tag{29}$$

D. Surrogate-Management Framework

A surrogate-management framework developed by authors (see [38]) is used for optimizing the control parameters of active flow control over an airfoil via a synthetic jet. The flowchart is illustrated in Fig. 2. The optimization procedure can be divided into several steps, as follows:

1) *Initialization:* Define the cost function (such as lift or drag coefficient) to be modeled and optimized, define the state functions and constraints, and specify the design space by defining the design variables and their range.

2) *Sampling:* According to the DOE method, the sample points and test points with the number of N and N_{test}, respectively, are chosen. For the problem with N_V design variables, let $\boldsymbol{x}_{S,i} = [x_{S,i}^1, x_{S,i}^2, \ldots, x_{S,i}^{N_V}]$ ($i \in \{1, 2, \ldots, N\}$) and $\boldsymbol{x}_{T,i} = [x_{T,i}^1, x_{T,i}^2, \ldots, x_{T,i}^{N_V}]$ ($i \in \{1, 2, \ldots, N_{\text{test}}\}$), respectively, denote the sample points and test points in design space.

3) *Sample-point evaluation:* By the time-accurate CFD analysis described in Sec. II, the aerodynamic performances $y_{S,i}$ at the sample points $\boldsymbol{x}_{S,i}$ and $y_{T,i}$ at test points$\boldsymbol{x}_{T,i}$ are calculated. Then the sampled data sets $\{(\boldsymbol{x}_{S,i}, y_{S,i}), i = 1, 2, \ldots, N\}$ and $\{(\boldsymbol{x}_{T,i}, y_{T,i}), i = 1, 2, \ldots, N_{\text{test}}\}$ are formed.

4) *Surrogate-model constructions:* Based on the sampled data sets, the approximation models $\hat{y}(\boldsymbol{x})$ are built (one for each fore coefficient). Several types of approximation models (such as RSM, kriging, RBF-NN model, etc.) are taken as the candidate models. The error estimation at the points $\boldsymbol{x}_{Ti}$ is performed to check the accuracy of the candidate models. The one with the best consistency between $\hat{y}(\boldsymbol{x})$ and y_{Ti} is adopted as the final surrogate model. If the accuracy of the surrogate model satisfies the requirement of a designer, one can turn into the next step; if not, switch to step 1 or build new surrogate models by tuning the parameters of the approximation models or adding more sample points to the DOE or redefining the optimization problem. The above steps are recursively performed until the

Table 2 Control parameters for test points

Sample point	C_μ	F^+	$\theta_{\text{jet}}/^\circ$.
1	0.00480	0.98000	45.00000
2	0.00860	1.50000	17.00000
3	0.02000	1.24000	31.00000
4	0.00100	0.46000	24.00000
5	0.01620	0.72000	10.00000
6	0.01240	0.20000	38.00000

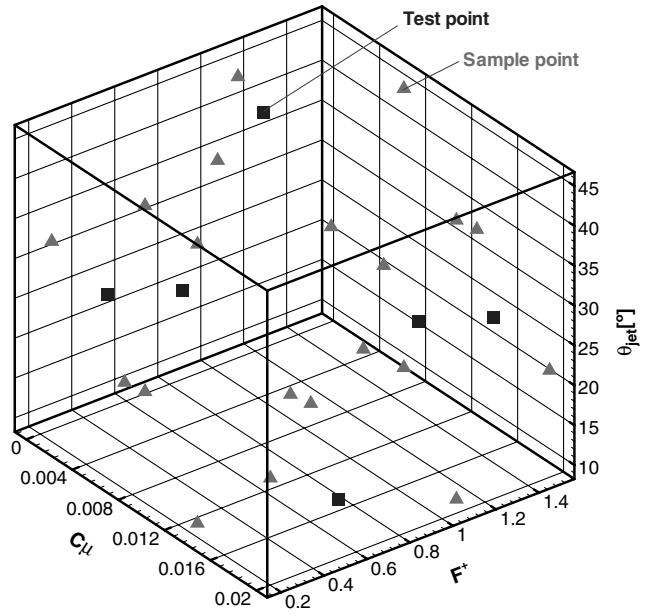

Fig. 8 Sample points and test points in design space.

accuracy is satisfactory. Note that in Fig. 2, the circled numbers 1–3 denote three ways to refine the model for improving the accuracy.

5) *Optimization and updating:* The selected surrogate model is coupled with an SAGA optimizer to obtain the global optimum that indicates the best control parameters. With the optimal control parameters, an extra time-accurate CFD simulation is performed to check the accuracy of the predicted optimum. If the accuracy of the predicted optimum is satisfactory, output the true optimum and terminate the whole process chain; if not, go back to step 4 and rebuild the surrogate model by augmenting the sampled data sets with the optimum.

IV. Results and Discussing

A. Validation of Flow Solver

The TAU 0015 airfoil is a modified NACA 0015 airfoil. The flow control over a TAU0015 airfoil [3] via a synthetic jet is numerically simulated to validate the time-accurate flow solver. The leading-edge geometry of a TAU0015 airfoil and the computational grid are shown in Figs. 3 and 4, respectively. The total number of grid cells is 344×96, and the first spacing of grid lines near the airfoil is $1.0 \times 10^{-6}c$ (c is the chord of an airfoil). The simulation is conducted with a Mach number of 0.15 and Reynolds number of 1.2×10^6. The synthetic jet works with a jet of width $h = 0.14\%c$, momentum coefficient $C_u = 0.03\%$, nondimensional frequency $F^+ = 0.58$, and jet angle $\theta_{\text{jet}} = 90°$. Figure 5 shows the comparison of the computed results and the experimental data for both the baseline and controlled cases. It is preliminarily shown that the flow solver is suitable for simulation of active flow control over an airfoil via a synthetic jet.

Table 3 Error estimation of approximation models

Approximation model	Average relative error $\bar{e}$	Root-mean-squared error σ_e
	Averaged C_l	
RSM	0.00744	0.00284
Kriging	0.00634	0.00364
RBF-NN	0.01489	0.00795
	Averaged C_d	
RSM	0.03474	0.02840
Kriging	0.03617	0.03492
RBF-NN	0.03641	0.01715
	Averaged C_m	
RSM	0.04597	0.04184
Kriging	0.04582	0.03720
RBF-NN	0.06733	0.04412

B. Optimizing a Synthetic Jet for Flow Control over a NACA 001 Airfoil

The developed method described in Sec. III is used to determine the optimal control parameters of a synthetic jet for aerodynamic stall control over a NACA 0015 airfoil. The baseline flow conditions are the same as those in the flow control experiments of Gilarranz et al. [7]. The chord Reynolds number is 8.95×10^5 and the Mach number is 0.1. The computational grid, shown in Fig. 6, is composed of 369×65 grid points, with 249 points on the upper surface of the airfoil and 41 points covering the jet orifice. The first spacing of grid lines near the airfoil is $1.0 \times 10^{-5}c$. The width of the jet orifice is $0.53\%c$, and the jet is located at $12\%c$ from the leading edge. The physical time step of the unsteady simulation is determined by dividing one period of synthetic-jet actuation into 72 physical steps. The number of subiterations for each physical time step is fixed to 20 multigrid cycles (100 iterations on fine grid). The simulation is performed within about 120 periods of the synthetic-jet actuation until the full periodic flow is observed. The first 60 periods of

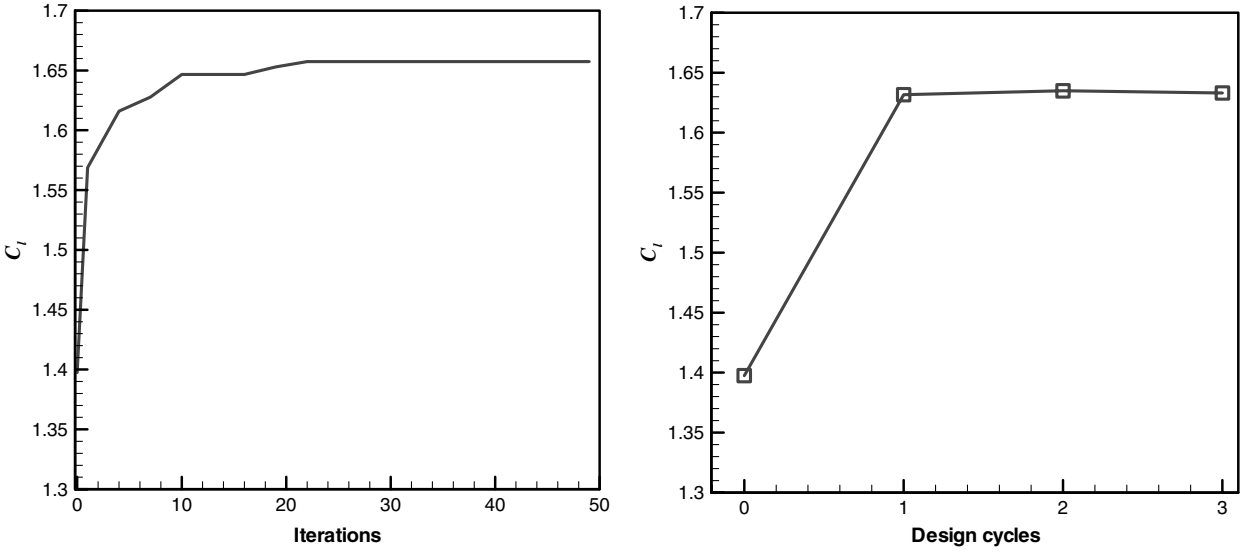

Fig. 9 Iteration history of optimization: a) convergence of SAGA for the first design cycle (lift by surrogate) and b) convergence of whole process (lift by CFD).

Table 4 Optimization results of active flow control over NACA 001 airfoil ($Ma = 0.1$, $\alpha = 16°$, and $Re = 8.96 \times 10^5$)

	C_μ	F^+	$\theta_{\text{jet}}/°$	C_l	C_d	C_m
Baseline	——	——	——	1.37269	0.04712	0.02924
Initial (0 cycle)	0.00800	1.00000	25.00000	1.39749	0.04125	0.02790
First cycle						
Optimum (surrogate)	0.02000	0.63084	10.00000	1.66819	0.03214	0.01882
Optimum (CFD)	0.02000	0.63084	10.00000	1.63166	0.03588	0.01768
Error for optimum	——	——	——	2.0%	11.6%	6.0%
Second cycle						
Optimum (surrogate)	0.02000	0.80808	10.62105	1.65097	0.03575	0.01798
Optimum (CFD)	0.02000	0.80808	10.62105	1.63490	0.03572	0.01748
Error for optimum	——	——	——	1.0%	0.1%	2.8%
Third cycle						
Optimum (surrogate)	0.02000	0.78062	11.21223	1.64401	0.03558	0.01742
Optimum (CFD)	——	——	——	1.63308	0.03573	0.01770
Error for optimum	——	——	——	0.7%	0.4%	1.6%

simulation are for the baseline simulation and the rest is for the flow control simulation. The averaging for the five periods was performed to obtain the averaged aerodynamic performances. A typical convergence history of the lift coefficient is illustrated in Fig. 7.

To obtain the optimal momentum coefficient C_μ, nondimensional frequency F^+ and jet angle θ_{jet} for maximizing the averaged lift coefficient, the mathematical model is established as

$$\begin{aligned} &\max\ C_l \\ &\text{subject to } |C_m| < 0.02 \\ &\quad 0.001 \le C_\mu \le 0.02 \\ &\quad 0.2 \le F^+ \le 1.5 \\ &\quad 10° \le \theta_{\text{jet}} \le 45° \end{aligned} \tag{30}$$

The optimization was first performed at the angle of attack of 16° (the critical angle of attack for baseline flow). Twenty sample points and six test points were chosen according to uniform design [37] of $U_{20}(4^3)$ and $U_6(6^3)$, respectively, listed in Tables 1 and 2. The sample points and test points are also shown in Fig. 8. Time-accurate CFD simulations were run at each sample point, and the corresponding aerodynamic data such as lift, drag, and moment coefficients were obtained. The CFD simulation can be performed on a number of personal computers, resulting in a simple but efficient parallel computation without need of communication between any two CPUs during computing. Since 13 personal computers equipped with Pentium 3.4 GHz processors were used, all the computations can be finished with 15 h. It took a total of about 120 h of elapsed CPU time. RSM, kriging, and RBF-NN models were built from sample points, and the error estimation was performed at the test points, as listed in Table 3. Note that for each force coefficient, one surrogate model should be built, as we assume that the outputs of RSM, kriging, or RBF-NN model are scalar. The comparison of the modeling error shows that RSM and kriging models have nearly identical accuracy. The kriging model was chosen as the surrogate model to be used in the optimization, as it is more reliable for problems with multiple extremes.

The chosen kriging model was coupled with a SAGA optimizer with population of 50, crossover probability of 0.5, mutation probability of 0.2, and maximum number of generations of 200. The SAGA optimization was terminated if there was no improvement of the objective function within a continuous 30 evolutions or the number of evolution reached the limitation of maximum number of generations. In SAGA optimization, the constraints were tackled by penalty function method. It took less than 1 min for each SAGA optimization with 60-generation evolutions, as the CFD analysis was completely replaced by a very efficient mathematic model (surrogate model). After SAGA optimization, an additional CFD calculation was performed to get the true values of C_l, C_d, and C_m using the optimal control parameters. Then the kriging model was refined by augmenting the sampled data sets with the optimum obtained by SAGA and evaluated by CFD. The whole process was run recursively for a few design cycles until convergence was observed. The convergence history of the objective function for the first design cycle and the whole process is shown in Figs. 9a and 9b, respectively. As a result of the optimization procedure, the lift coefficient is increased by 16.9% and the drag coefficient (due to flow separation) is reduced by 13.4% with respect to the initial controlled flow, as illustrated in Table 4. Figure 10 shows the averaged flowfields near the trailing edge of a NACA 0015 airfoil without and with the flow controls using initial and optimal control parameters. For the flow control with initial control parameters, little effect can be found for separation suppression; when optimal control parameters were used, the separation region was nearly eliminated.

The optimization of the control parameters was then performed for different angles of attack using the same strategy discussed above. The results for angles of attack from 14 to 22° are shown in Fig. 11. The optimal results were compared with baseline data and also with those using initial control parameters ($c_\mu = 0.008$, $F^+ = 1$, and $\theta_{\text{jet}} = 25°$). This comparison shows that the stall performances such

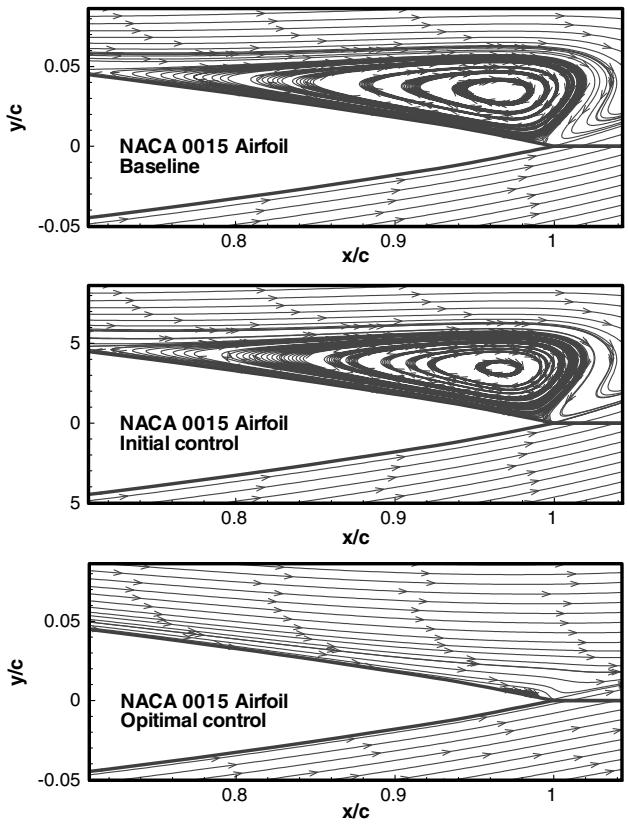

Fig. 10 Comparison of averaged flowfields near the trailing edge without and with controls using initial and optimal parameters.

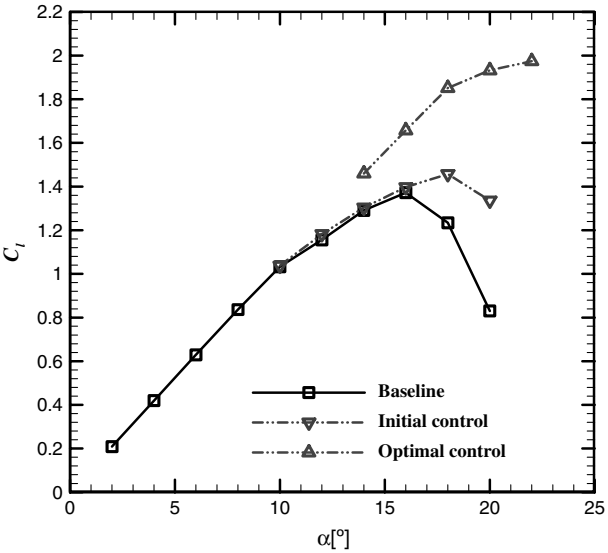

Fig. 11 Optimal results of lift curve for different angles of attack.

as the lift slope before stall, the critical angle of attack, maximum lift coefficient, etc., were remarkably improved as a result of the optimization procedure. Note that we only take a 2-D simulation of flow control via a synthetic jet as an example to demonstrate and evaluate the feasibility and efficiency of the developed surrogate-based optimization methods. For a more realistic problem, 3-D simulation is preferred for checking the results of optimization. However, it is beyond the scope of this paper.

V. Conclusions

A surrogate-based optimization method has been developed to address the high computational effort associated with the optimization of active stall control via a synthetic jet. This method was demonstrated and evaluated for optimizing the actuation parameters of a synthetic jet for active stall control over a NACA 0015 airfoil. Significantly improved aerodynamic performance has been observed. The preliminary conclusions for this method can be drawn as follows:

1) The surrogate-model methods used in this paper are accurate and engineering-usable for the modeling of the aerodynamic data of an airfoil controlled by a synthetic jet.

2) The difficulty of directly coupling the time-accurate CFD simulation and genetic algorithm optimizer can be avoided by replacing the time-consuming CFD simulation with a surrogate model within a surrogate-management framework.

Future research work includes the optimization of the location of synthetic jet, application to multijet flow control, and extension of the current method to 3-D active flow control via a synthetic jet.

Acknowledgments

This research has benefited greatly from the support of the National Natural Science Foundation of China under grant no. 10702055 and grant no. 10902088.

References

[1] Collis, S. S., Joslin, R. D., Seifert, A., and Theofilis, V., "Issues in Active Flow Control: Theory, Control, Simulation, and Experiment," *Progress in Aerospace Sciences*, Vol. 40, No. 4-5, 2004, pp. 237–289. doi:10.1016/j.paerosci.2004.06.001

[2] Smith, B. L., and Glezer, A., "Vectoring and Small-Scale Motions Effected in Free Shear Flows Using Synthetic Jet Actuators," 35th AIAA Aerospace Sciences Meeting, AIAA Paper 97-0213, 1997.

[3] Seifert, A., Darabi, A., and Wyganski, I., "Delay of Airfoil Stall by Periodic Excitation," *Journal of Aircraft*, Vol. 33, No. 4, 1996, pp. 691–697. doi:10.2514/3.47003

[4] Hites, M., Nagib, H., Bachar, T., and Wygnanski, I., "Enhanced Performance of Airfoils at Moderate Mach Numbers Using Zero-Mass Flux Pulsed Blowing," 39th Aerospace Sciences Meeting and Exhibit, AIAA Paper 2001-0734, 2001.

[5] Amitay, M., Smith, D. R., Kibens, V., Parekh, D. E., and Glezer, A., "Aerodynamic Flow Control over an Unconventional Airfoil Using Synthetic Jet Actuators," *AIAA Journal*, Vol. 39, No. 3, 2001, pp. 361–370. doi:10.2514/2.1323

[6] Hassan, A. A., and Munts, E. A., "Transverse and Near-Tangent Synthetic Jets for Aerodynamic Flow Control," 18th Applied Aerodynamics Conference, AIAA Paper 2000-4334, 2000.

[7] Gilarranz, J. L., Traub, L. W., and Rediniotis, O. K., "Characterization of a Compact, High Power Synthetic Jet Actuator for Flow Separation Control," AIAA Paper 2002-0127, 2002.

[8] McCormick, D. C., "Boundary Layer Separation Control with Directed Synthetic Jets," 38th Aerospace Sciences Meeting & Exhibit, AIAA Paper 2000-0519, 2000.

[9] Smith, B. L., and Glezer, A., "Vectoring of a High Aspect Ratio Rectangular Air Jet Using a Zero Net-Mass-Flux Control Jet," *Bulletin of the American Physical Society*, Vol. 39, p. 1994.

[10] Chen, Y. L., Liang, S., Aung, K., and Glezer, A., "Enhanced Mixing in a Simulated Combustor Using Synthetic Jet Actuators," AIAA Paper 99-0449, 1999.

[11] Chen, F. J., and Beeler, G. B., "Virtual Shaping of a Two-Dimensional NACA 0015 Airfoil Using Synthetic Jet Actuator," AIAA Paper 2002-3273, 2002.

[12] Roos, F. W., "Synthetic-Jet Microblowing for Forebody Flow-Asymmetry Management," AIAA Paper 98-0212, 1998.

[13] Hassan, A. A., "Numerical Simulations and Potential Applications of Zero-Mass Jets for Enhanced Rotorcraft Aerodynamic Performance," AIAA Paper 98-0211, 1998.

[14] Nagib, H., Greenblatt, D., Kiedaisch, J., Wygnanski, I., and Hassan, A., "Effective Flow Control for Rotorcraft Applications at Flight Mach Numbers," AIAA Paper 2001-2974, 2001.

[15] Lorber, P. F., McCormick, D. C., Anderson, T. J., Wake, B. W., MacMartin, D. G., Pollack, M. J., Corke, T. C., and Breuer, K., "Rotorcraft Retreating Blade Stall Control," AIAA Paper 2000-2475, 2002

[16] Amitay, M., Washburn, A. E., Anders, S. G., and Parekh, D. E., "Active Flow Control on the Stingray UAV: Transient Behavior," *AIAA Journal*, Vol. 42, No. 11, 2004, pp. 2205–2215. doi:10.2514/1.5697

[17] Wu, J. Z., Lu, X. Y., Denny, A. G., Fan, M., and Wu, J. M., "Post-Stall Flow Control on an Airfoil by Local Unsteady Forcing," *Journal of Fluid Mechanics*, Vol. 371, 1998, pp. 21–58.

[18] Donovan, J. F., Kral, L. D., and Cary, A. W., "Active Flow Control Applied to an Airfoil," 36th AIAA Aerospace Sciences Meeting, AIAA Paper 98-0210, 1998.

[19] Hassan, A. A., "Oscillatory and Pulsed Jets for Improved Airfoil Aerodynamics—A Numerical Simulation," 42nd AIAA Aerospace Sciences Meeting and Exhibit, AIAA Paper 2004-0227, 2004.

[20] Rumsey, C. L., Gatski, T. B., Sellers, W. L., Vatsa, V. N., and Viken, S. A., "Summary of the 2004 CFD Validation Workshop on Synthetic Jets and Turbulent Separation Control," AIAA Paper 2004-2217, 2004.

[21] Duvigneau, R., and Visonneau, M., "Optimization of a Synthetic Jet Actuator for Aerodynamic Stall Control," *Computers & Fluids*, Vol. 35, No. 6, 2006, pp. 624–638. doi:10.1016/j.compfluid.2005.01.005

[22] Duvigneau, R., and Visonneau, M., "Simulation and Optimization of Stall Control for an Airfoil with a Synthetic Jet," *Aerospace Science and Technology*, Vol. 10, No. 4, 2006, pp. 279–287. doi:10.1016/j.ast.2006.01.002

[23] Duvigneau, R., Hay, A., and Visonneau, M., "Optimal Location of a Synthetic Jet on an Airfoil for Stall Control," *Journal of Fluids Engineering*, Vol. 129, No. 7, 2007, pp. 825–833. doi:10.1115/1.2742729

[24] Liou, M. S., "A Sequel to AUSM, Part 2: AUSM$^+$-up for All Speeds," *Journal of Computational Physics*, Vol. 214, No. 1, 2006, pp. 137–170. doi:10.1016/j.jcp.2005.09.020

[25] Turkel, E., Radespiel, R., and Vatsa, V. N., "Preconditioning Methods for Low Speed Flows," AIAA Paper 96-2460, 1996.

[26] Xie, F.-T., Song, W.-P., and Han, Z.-H., "Numerical Study of High-Resolution Scheme Based on Preconditioning Method," *Journal of Aircraft*, Vol. 46, No. 2, 2009, pp. 520–525. doi:10.2514/1.37976

[27] Han, Z.-H., He, F., Song, W.-P., and Qiao, Z.-D., "A Preconditioned

Multigrid Method for Efficient Simulation of Three-Dimensional Compressible and Incompressible Flows," *Chinese Journal of Aeronautics*, Vol. 20, No. 4, 2007, pp. 289–296.
doi:10.1016/S1000-9361(07)60046-6

[28] Han, Z.-H., Qiao, Z.-D., and Song, W.-P., "Numerical Simulation of Active Flow Control to Airfoil Stall Using Local Synthetic Jet," *Acta Aeronautica et Astronautica Sinica*, Vol. 28, No. 5, 2007, pp. 1040–1046 (in Chinese).

[29] Koch, P. N., Simpson, T. W., Allen, J. K., and Mistree, F., "Statistical Approximations for Multidisciplinary Design Optimization: The Problem of the Size," *Journal of Aircraft*, Vol. 36, No. 1, 1999, pp. 275–286.
doi:10.2514/2.2435

[30] Rodriguez, D. L., and Stanford, C. A., "Response Surface Based Optimization with a Cartesian CFD Method," AIAA Paper 2003-0465, 2003.

[31] Sacks, J., Welch, W. J., Mitchell, T. J., and Wynn, H. P., "Design and Analysis of Computer Experiments," *Statistical Science*, Vol. 4, No. 4, 1989, pp. 409–423.
doi:10.1214/ss/1177012413

[32] Simpson, T. W., Mauery, T. M., Korte, J. J., and Mistree, F., "Kriging Models for Global Approximation in Simulation-Based Multidisciplinary Design Optimization," *AIAA Journal*, Vol. 39, No. 12, 2001, pp. 2233–2241.
doi:10.2514/2.1234

[33] Martin, J. D., and Simpson, T. W., "Use of Kriging Model to Approximate Deterministic Computer Models," *AIAA Journal*, Vol. 43, No. 4, 2005, pp. 863–863.
doi:10.2514/1.8650

[34] Park, J., and Sandberg, I. W., "Universal Approximation Using Radial-Basis-Function Networks," *Neural Computation*, Vol. 3, No. 2, 1991, pp. 246–257.
doi:10.1162/neco.1991.3.2.246

[35] Elanayar, S. V. T., and Shin, Y. C., "Radial Basis Function Neural Network for Approximation and Estimation of Nonlinear Stochastic Dynamic Systems," *IEEE Transactions on Neural Networks*, Vol. 5, No. 4, 1994, pp. 594–603.
doi:10.1109/72.298229

[36] Giunta, A. A., Wojtkiewicz, S. F., Jr., and Eldred, M. S., "Overview of Modern Design of Experiments Methods for Computational Simulations," AIAA Paper 2003-649, 2001.

[37] Fang, K. T., Lin, D., Winker, P., and Zhang, Y., "Uniform Design: Theory and Application," *Technometrics*, Vol. 42, No. 3, 2000, pp. 237–248.
doi:10.2307/1271079

[38] Zhang, K.-S., Han, Z.-H., Li, W.-J., and Song, W.-P., "Coupled Aerodynamic/Structural Optimization of a Subsonic Transport Wing Using a Surrogate Model," *Journal of Aircraft*, Vol. 45, No. 6, 2008, pp. 2167–2171.
doi:10.2514/1.36047